Face Verification Across Age Progression

Narayanan Ramanathan, *Student Member, IEEE*, and Rama Chellappa, *Fellow, IEEE*

***Abstract*—Human faces undergo considerable amounts of variations with aging. While face recognition systems have been proven to be sensitive to factors such as illumination and pose, their sensitivity to facial aging effects is yet to be studied. How does age progression affect the similarity between a pair of face images of an individual? What is the confidence associated with establishing the identity between a pair of age separated face images? In this paper, we develop a Bayesian age difference classifier that classifies face images of individuals based on age differences and performs face verification across age progression. Further, we study the similarity of faces across age progression. Since age separated face images invariably differ in illumination and pose, we propose preprocessing methods for minimizing such variations. Experimental results using a database comprising of pairs of face images that were retrieved from the passports of 465 individuals are presented. The verification system for faces separated by as many as nine years, attains an equal error rate of 8.5%.**

***Index Terms*—Age progression, face recognition, face verification, probabilistic eigenspaces, similarity measure.**

I. Introduction

PERCEIVING human faces and modeling the distinctive features of human faces that contribute most towards face recognition are some of the challenges faced by computer vision and psychophysics researchers. Human faces belong to a special class of 3-D objects, modeling which involves developing accurate characterizations that account for illumination, head pose variations, facial expressions, etc. Moreover, human faces also undergo growth related changes that are manifested in the form of shape and textural variations. Hence, the robustness to variations due to factors such as illumination, pose, facial expressions, aging, etc., is a significant metric in evaluating face recognition systems. Over the years, many still-image and video based face recognition algorithms have been developed. Zhao *et al.* [2] provide a thorough qualitative analysis of the many different face recognition algorithms. Recently, good to very good recognition performance across illumination and pose variations were demonstrated by Zhang and Samaras [3] and Zhou and Chellappa [4], Blanz and Vetter [5], Georghiades *et al.* [6], and Gross *et al.* [7]. Moreover, many approaches have been proposed for modeling facial expressions. Facial Action Coding systems [8] have contributed significantly towards characterizing facial expressions. Yacoob and Davis [9], Essa and Pentland [10], Martinez [11], Tian *et al.* [12], and Liu *et al.* [13] have proposed approaches for identifying facial expressions from face images. Decades of dedicated research coupled with the advent of standardized performance evaluation protocols such as FERET [14], [15], and FRVT [16] have enhanced the commercial significance of face recognition systems.

Though psychophysical studies have contributed significantly towards the perception of growing faces and towards understanding craniofacial growth, age progression in human faces has largely been ignored while developing face recognition systems. Modeling age progression in human faces is a very challenging task. Facial aging effects are manifested in different forms in different age groups. While aging effects are often manifested in the form of shape variations in human faces due to the cranium's growth from infancy to teen years [17], they are more commonly observed in the form of textural variations such as wrinkles and other skin artifacts in adult faces. Apart from biological factors, factors such as climatic conditions, ethnicity, mental stress, etc., are often attributed to play a role in the process of aging. Some of the interesting applications of studying age progression in human faces are discussed as follows.

- Developing face recognition systems that are robust to age progression would enable the successful deployment of face recognition systems in public places. Such systems would be highly beneficial to homeland security applications. Further, developing systems that verify face images across age progression would annul the necessity of periodically updating large face databases with more recent images.
- Since different individuals age differently, developing automatic age progression systems that could predict the many different ways a person could have aged would have a significant impact in finding missing individuals.
- Ethological studies have revealed that the perceived age of an individual significantly affects the type and amount of behavior directed towards him/her by other individuals. Hence, building systems that could reliably estimate the age of individuals, would be useful for developing human-robot interaction systems and human-computer interaction systems.
- Changes in facial appearances are attributed to have a significant psychosocial impact on an individual [17]. Studies related to craniofacial growth are bound to help surgeons and orthodontists in treating disfigurements and deformities in faces.

Before we formulate the problem, we provide a brief overview of the previous work on age progression in human faces.

Manuscript received October 14, 2005; revised April 17, 2006. A portion of the work presented in this paper was presented at the IEEE Conference on Computer Vision and Pattern Recognition. This work was supported in part by a fellowship from P. Horvitz (Apptis, Inc.). The associate editor coordinating the review of this manuscript and approving it for publication was Dr. Ercan E. Kuruoglu.

N. Ramanathan is with the Department of Electrical and Computer Engineering, University of Maryland, College Park, MD 20742-3275 USA (e-mail: ramanath@umiacs.umd.edu).

R. Chellappa is with the Center for Automation Research (CfAR) and the Department of Electrical and Computer Engineering, University of Maryland, College Park, MD 20742-3275 USA (e-mail: rama@umiacs.umd.edu).

Color versions of Figs. 5, 8, and 9 are available online at http://ieeexplore.ieee.org.

Digital Object Identifier 10.1109/TIP.2006.881993

A. Previous Work on Age Progression

Gibson's ecological approach towards perception [18] and Thompson's [19] pioneering work on geometric transformations in the study of morphogenesis largely laid the foundations for the study of craniofacial growth. Since then, many of Thompson's approaches to morphogenesis have been adopted to describe the process of craniofacial growth. Shaw *et al.* [20] proposed the cardioidal strain transformation for global remodeling of the human skull. Pittenger and Shaw [21] studied aging faces as a series of viscal-elastic events. They analyzed the relative importance of three characteristic patterns of growth in human faces, namely, shear, strain, and radial growth, on the perceived age of faces and observed that cardioidal strain transformations had the maximum impact in affecting the perceived age of faces. Todd *et al.* [22] proposed the "revised" cardioidal strain transformation model for craniofacial growth. They treated the human head as a fluid filled spherical water tank and performed a hydrostatic analysis on the effects of gravity on craniofacial growth. Their hypothesis was in accordance with Wolff's Law that attributes stress as a direct stimulant to growth and proposes that a growing structure changes in accordance with the amount and direction of stress acting on it.

Psychophysical evidences collected on age progression in human faces have formed the basis for some of the recent works in this topic. In computer vision, age progression in human faces has been studied from two perspectives: one towards developing automatic age estimation techniques to classify face images based on age and the other towards developing automatic age progression systems to perform face recognition age progression. Kwon *et al.* [23] developed a system that classifies face images into one of three age groups: infants, young adults and senior adults. Based on the ratios of distances between key landmarks extracted from face images, they classified face images as that of infants or adults. They also proposed methods to detect wrinkles in predesignated regions in face images to further classify adult images into young adults and senior adults. Lanitis *et al.* [24] proposed methods to simulate aging effects on face images. They developed an aging function that is based on a parametric model of face images and performed tasks such as automatic age estimation, face recognition across age progression, etc. Their database comprised of face images of individuals under 30 years of age. Further, Lanitis *et al.* [25] performed a quantitative evaluation of the performance of different classifiers for the task of automatic age estimation. They evaluated classifiers based on supervised and unsupervised neural networks and the minimum distance classifier for the task of automatic age estimation.

Burt and Perrett [26] created facial prototypes for different age groups by averaging the shape and texture of faces that belong to their respective age groups. They studied the variations between facial prototypes of different age groups and observed that by incorporating such variations in faces, the perceived age of faces changed, but such facial prototypes were observed to be ineffective in capturing wrinkles that are characteristic of elderly subjects. Tidderman *et al.* [27] extended the above approach by compensating for the loss of texture in the facial prototypes that occurred during the blending process. Using wavelet-based methods they created texture enhanced prototypes by adjusting the amplitude of edges in the composite image. Following the shape and texture transformations described in [26], they transformed the texture of face images using locally weighted wavelet functions at different scales and orientations and thereby increased the perceived age of a face image.

Wu *et al.* [28] represented skin deformations as a plastic-visco-elastic process and generated permanent wrinkles through a simulation of inelastic skin deformations. O'Toole *et al.* [29] applied a standard facial caricaturing algorithm to 3-D models of faces and reported an increase in the perceived age of faces when facial creases were exaggerated into wrinkles and a decrease in the perceived age, when such creases were de-emphasized. Gandhi [30] designed a support vector machine (SVM) based age prediction function and extended the image based surface detail transfer approach [31] towards emphasizing or de-emphasizing wrinkles on face images. Givens *et al.* [32] analyzed the role of various co-variates such as age, gender, expression, facial hair, etc., in affecting the performance of three face recognition algorithms and noted that older faces were often easier to recognize than younger faces.

B. Problem Statement

While face images have traditionally been used in identification documents such as passports, driver's licenses, voter ID, etc., in recent years, face images are being increasingly used as additional means of authentication in applications such as credit/debit cards and in places of high security. Since faces undergo gradual variations due to aging, periodically updating face databases with more recent images of subjects might be necessary for the success of face recognition systems. Since periodically updating such large databases would be a tedious task, a better alternative would be to develop face recognition systems that verify the identity of individuals from a pair of age separated face images. Understanding the role of age progression in affecting the similarity between two face images of an individual is important in such tasks.

We wish to address the following problem: How similar is a pair of age separated face images of an individual? How do inherent changes in a human face due to aging, affect facial similarity? Given a pair of age separated face images of an individual, what is the confidence measure associated with verifying his/her identity? Our database comprises of pairs (younger and most recent) of face images retrieved from the passports of 465 individuals. Table I summarizes the database. The age span of individuals in our database is 20 years to 70 years. Fig. 1 shows a few sample images from our database.

Though passport images are generally taken under controlled environments, subtle variations in head pose tend to exist and hence face images are not strictly frontal in pose. Further, we observed many instances where passport images were taken under nonuniform illumination conditions. To study age progression in human faces, it is crucial to reduce variations due to factors such as head pose and illumination. In Section II, we propose methods to recover a frontal face from nonfrontal face images

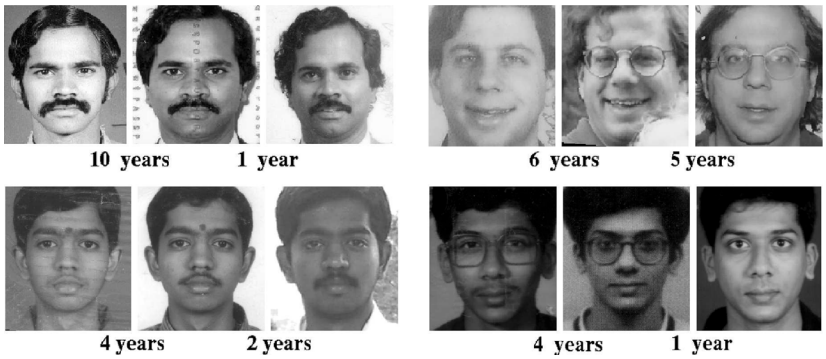

Fig. 1. Some sample age-separated images of individuals retrieved from their passports.

TABLE I
DATABASE OF PASSPORT IMAGES

Age Difference	No: of image pairs
1-2 yrs	165
3-4 yrs	104
5-7 yrs	81
8-9 yrs	115

and to correct for nonuniform illumination on faces. In Section III, we build a Bayesian age-difference classifier that verifies the identity between a pair of age separated face images and estimates the age difference between a pair of face images. In Section IV, we study the similarity of faces across age progression and highlight some of the interesting results obtained using the proposed similarity measure. Section V discusses some directions for future work.

II. Pose Correction and Illumination Compensation

A. Frontal Face Recovery

In this section, we propose a method to recover the frontal face of an individual from a nonfrontal face image. Blanz and Vetter, in their seminal work on 3-D morphable models for faces [33], [5], estimate the 3-D shape and texture of faces from a single face image and perform face recognition across varying pose and illumination. Our method draws inspiration from their work. But the computational simplicity of our method coupled with the need for very little manual intervention, if any, makes our approach more suitable to the recovery of frontal faces from nonfrontal passport images. Head pose orientations are generally described using three angles, namely, pitch, yaw, and roll. Though pose variations in passport images are generally small, in our dataset we observed that the face orientations described by the yaw angle were significantly different from that of frontal faces. Hence, we focus on recovering the frontal face from face images where the yaw angle is nontrivial. The method is trivially extendable to pose correction on rotations about the other two axes. Our approach is described in detail, below.

Our training set comprises of 3-D head scans of 100 faces. Let $S_1, S_2, \ldots\ldots, S_{100}$ and $T_1, T_2, \ldots\ldots T_{100}$ be the corresponding shape and texture vectors extracted from the 3-D head scans of the 100 faces. The shape vector $S = (x_1, y_1, z_1, \ldots\ldots, x_N, y_N, z_N)^T$ represents the (x, y, z) coordinates of N vertices and the texture vector $T = (t_1, t_2, \ldots t_N)^T$ represents the grayscale intensities at the N corresponding vertices. Let R_θ correspond to the rotation matrix for a yaw angle θ. The 3-D faces are rotated by different angles θ and the corresponding textures are extracted by appropriately mapping the frontal face textures to faces rotated by such angles. Let f be the function that maps frontal face textures to faces in different orientations and let $T_i^{(\theta)}, i = 1, 2, \ldots, 100$ correspond to the texture of faces from the training set, rotated by a yaw angle θ. $T_i^{(\theta)}$, $i = 1, 2, \ldots, 100$ can be computed as below. In (1), P corresponds to the orthographic projection matrix

$$\begin{aligned} s_i^{(\theta)} &= P R_\theta S_i \\ T_i^{(\theta)} &= f(T_i, s_i^{(\theta)}). \end{aligned} \tag{1}$$

There exists an underlying correlation between the shape of a face and the corresponding facial texture. Our approach is based on exploiting the underlying correlation between the two attributes. We apply the principal component analysis [34] on the texture $\{T^{(\theta)}\}_{i=1}^N$ and shape vectors $\{S_i\}_{i=1}^N$ and construct their respective eigenspaces. Let the eigenvectors of the texture space $\mathbf{T}^{(\theta)}$ and shape space $\mathbf{S}$ be $\Phi^{(\theta)} = (\phi_1^{(\theta)}, \phi_2^{(\theta)}, \ldots\ldots, \phi_N^{(\theta)})$ and $\Psi = (\psi_1, \psi_2, \ldots\ldots, \psi_N)$, respectively. By projecting the shape and texture vectors at different orientations onto their respective eigenspaces, we represent them by means of their principal components

$$T_i^{(\theta)} = \bar{T}^\theta + \sum_{j=1}^{N} \alpha_{ij}^{(\theta)} \phi_j^{(\theta)} \quad i \in (1, 2, \ldots, N) \tag{2}$$

$$S_i = \bar{S} + \sum_{j=1}^{N} \beta_{ij} \psi_j \quad i \in (1, 2, \ldots, N). \tag{3}$$

Hence, each pair of texture and shape vector of a face $[(T_1^{(\theta)}, S_1), (T_2^{(\theta)}, S_2), \ldots\ldots (T_N^{(\theta)}, S_N)]$ is represented by its principal component vector pairs $[(\underline{\alpha}_1^{(\theta)}, \underline{\beta}_1), (\underline{\alpha}_2^{(\theta)}, \underline{\beta}_2), \ldots\ldots (\underline{\alpha}_N^{(\theta)}, \underline{\beta}_N)]$. We assume that the principal components from the respective spaces are jointly Gaussian and estimate the joint probability distribution $p(\underline{\alpha}^\theta, \underline{\beta}|\theta)$.

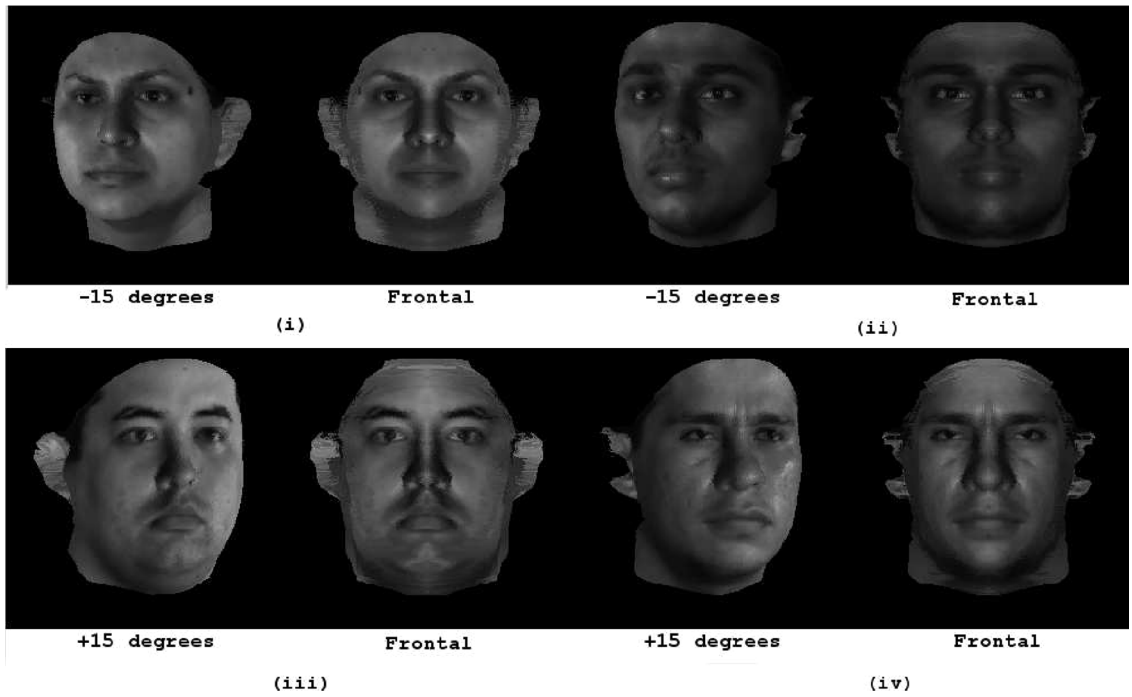

Fig. 2. Recovery of frontal faces: Images in the top and bottom rows illustrate the recovery of frontal faces from nonfrontal faces with a yaw $= -15^\circ$ and yaw $= +15^\circ$, respectively.

Next, given a nonfrontal color image I of an individual, we extract the face region using statistical color models for skin detection [35]. Using a large number of images on which skin and nonskin regions had been manually selected, we construct skin and nonskin histogram models and design a Bayes classifier [34] to perform skin detection. Let s[rgb] and n[rgb] be the pixel counts for skin and nonskin histograms respectively and T_s and T_n, the total pixel counts in the skin and nonskin histograms respectively. The probabilities are defined as

$$P(\text{rgb}|\text{skin}) = \frac{s[\text{rgb}]}{T_s} \qquad P(\text{rgb}|\sim \text{skin}) = \frac{n(\text{rgb})}{T_n} \quad (4)$$

$$P(\text{skin}|rgb) = \frac{P(\text{rgb}|\text{skin})P(\text{skin})}{P(\text{rgb})}. \quad (5)$$

The detected skin region in the input image serves as a cue to estimate the scale of the input image. To estimate the head pose of the input image, we align the grayscale input image I_{gray} with an appropriately scaled average face $\bar{T}^{\theta}$ about their nose locations and compute the disparity between their edge maps I_e and $\bar{T}_e^{\theta}$ respectively. The orientation θ that minimizes the disparity between the edge maps serves as an estimate of the head pose. Since head pose variations in passport images tend to be small, we limit our search space to the range (-10° to $+10^\circ$)

$$\tilde{\theta} = \arg\min_{\theta} \left\| I_e - \bar{T}_e^{\theta} \right\|. \quad (6)$$

Having estimated the pose of the input image as $\tilde{\theta}$, the input image is projected on the texture space $\mathbf{T}^{(\tilde{\theta})}$ spanned by $\Phi^{(\tilde{\theta})}$ and the principal components on the texture space are computed. The principal components on the shape space $\mathbf{S}$ are subsequently estimated as illustrated as follows:

$$\underline{\alpha}_I^{\tilde{\theta}} = \left\langle I_{gray} - \bar{T}^{\theta}, \Phi^{(\tilde{\theta})} \right\rangle \quad (7)$$

$$\underline{\beta}_I = E(p(\beta|\underline{\alpha}_I^{\tilde{\theta}}, \tilde{\theta})). \quad (8)$$

Having estimated $\underline{\beta}_I$, we compute the 3-D shape of the input face image and recover the frontal face image

$$S_I = \bar{S} + \sum_{j=1}^{N} \beta_{I,j}\psi_j \quad (9)$$

$$I_{\text{frontal}} = f^{-1}(I_{gray}, PR_{\tilde{\theta}}S_I). \quad (10)$$

To illustrate the performance of our method, we generated nonfrontal images of four individuals from our training set at orientations -15° and $+15^\circ$. For this experiment, the training set that was used to create the eigenspaces comprised of shape and texture of the remaining 96 individuals from the original training set. Fig. 2 shows the recovered frontal face images corresponding to the four nonfrontal faces. Accurate face localization is a key to the success of our method. Since the eigenspaces for shape and texture can be computed off-line, the method is computationally simple. The presence of dark glasses or facial hair affects pose estimation and hence affects the performance of our method.

B. Illumination Compensation

While most face recognition systems perform commendably well on faces taken under uniform illumination conditions, their

TABLE II
EVALUATION OF HALF-FACES: RANK 1 RECOGNITION SCORE USING EIGENFACES ON FULL FACES AND HALF-FACES

Half-faces vs Full faces [a]: Rank 1 recognition scores (%)										
Gallery		f_{02}	f_{03}	f_{04}	f_{05}	f_{10}	f_{13}	f_{15}	f_{16}	f_{22}
Probes	f_{02}	-	c{97}	93{60}	38{29}	41{26}	29{4}	38{3}	35{3}	32{4}
	f_{03}	99{c}	-	c{c}	60{38}	62{41}	43{4}	41{3}	38{3}	46{3}
	f_{04}	72{44}	c{91}	-	c{84}	97{79}	56{4}	51{1}	40{1}	57{3}
	f_{05}	29{12}	47{21}	99{41}	-	c{c}	50{6}	37{4}	26{1}	51{6}
	f_{10}	26{10}	54{16}	97{49}	c{c}	-	56{6}	37{4}	18{4}	51{6}
	f_{13}	21{3}	41{3}	51{7}	53{6}	65{7}	-	97{68}	57{32}	c{c}
	f_{15}	44{3}	51{4}	51{4}	28{4}	26{4}	99{90}	-	97{82}	c{c}
	f_{16}	46{3}	46{4}	32{4}	18{4}	22{4}	82{49}	99{96}	-	90{65}
	f_{22}	29{3}	46{3}	54{4}	49{6}	37{7}	99{c}	c{c}	66{47}	-
Mean		46{22}	61{30}	72{54}	56{34}	56{34}	64{33}	63{35}	47{22}	66{36}

[a]Scores within {} are rank 1 recognition scores using full faces. In the table, entry 'c' corresponds to 100% recognition rates

Fig. 3. Images of an individual under each of nine different illumination conditions from the PIE dataset [43]. With images from each of $f_i, \mathrm{i} \in 02, 03, \ldots 22$ as the gallery and images from f_j, and $\mathrm{j} \neq \mathrm{i}$ as the probe, a round-robin recognition experiment was performed.

performance drops when presented with faces that were nonuniformly illuminated. Belhumeur *et al.* [36] discuss subspace methods for face recognition and cite that ignoring the first few principal components improves recognition performance in the presence of nonuniform illumination. Georghiades *et al.* [6] proposed the illumination cone model for face recognition. From a set of training images for each face, 3-D models are reconstructed and subsequently used to create synthetic images of faces under different illumination conditions and poses. The Lambertian surface approximation of faces enables the illumination cone to be well-approximated by a low-dimensional linear subspace. Basri and Jacobs [37] have shown that the set of images of a convex Lambertian object under arbitrary illumination conditions can be approximated by a low-dimensional linear subspace. They construct the spherical harmonic basis images for faces and subsequently propose a simple scheme to perform face recognition. Lee *et al.* [38] proposed an effective approximation to the basis images using nine single light source images of a face and reported good recognition performance. Recently, Aggarwal and Chellappa [39] proposed methods to perform face recognition in the presence of multiple light sources.

However, most of these approaches need a set of training images for each subject or 3-D scans of the subjects in the database. Real-life face images often contain specular reflections and hence, do not strictly exhibit the properties of a Lambertian surface. In the case of face images retrieved from passports, neither are multiple face images per subject available nor are the face images free from specular reflections. The nonuniformity in illumination in passport images is often due to imbalances in the illumination on either sides of the face. Self-shadows and specular reflections are some of the most common effects of uncontrolled illumination on faces. Given the aforementioned constraints, we propose a simple approach towards circumventing nonuniform illumination in face images retrieved from passports. We assume that faces are bilaterally symmetric and represent nonuniformly illuminated faces with the better illuminated half and discard the poorly illuminated half. Bilateral symmetry of human faces has been used earlier in SFS problems [40]. Further, psychophysical experiments conducted by Troje and Bulthoff [41] illustrate the role of bilateral symmetry of human faces in recognizing faces across novel views. On the contrary, Liu *et al.* [13] and Martinez [42] studied the asymmetries in either halves of the human face and used the same for studying facial expressions.

From a recognition perspective, how effective is the assumption of bilateral symmetry of human faces to circumvent nonuniform illumination across faces? To answer this question, we performed an eigenface based recognition experiment on the PIE dataset [43]. The details of the experiments are as follows: Frontal faces of 68 individuals in nine different illumination conditions $(f_{02}, f_{03}, f_{04}, f_{05}, f_{10}, f_{13}, f_{15}, f_{16}, f_{22})$ under the PIE nomenclature, were selected. Face recognition is performed in a round-robin fashion (f_i comprises the gallery set and f_j, $i \neq j$ comprises the probe set) and the performance of full-faces as against better illuminated half-faces was studied. The eigenspaces for full-faces and half-faces were created using well illuminated frontal face images from the Yale Face Database B [6]. Table II reports the rank 1 recognition scores under both the settings. Fig. 3 shows the face images from each of the nine illumination conditions. The nontrivial improvement in recognition performance on experiments such as (f_{04} versus f_{13}), (f_{10} versus f_{13}) illustrate the effectiveness of the proposed approach in challenging environments.

For the verification problem, we illustrate the significance of half-faces in computing a similarity measure on images of an

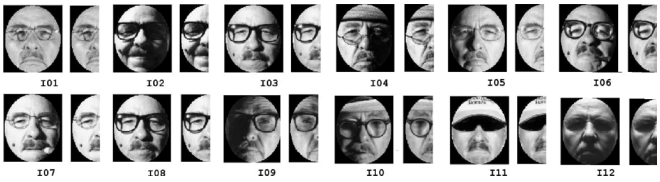

Fig. 4. Facial similarity experiment: Images of an individual taken under different illumination conditions and their corresponding half faces with better illumination.

TABLE III
FACIAL SIMILARITY SCORES: SET I CORRESPONDS TO FULL FACES AND SET II CORRESPONDS TO HALF-FACES FACES

Similarity Score(I_{01}, I_n)			
Image	Set I	Set II	Remark
I_{02}	-0.43	0.33	half-faces in set II perform better
I_{03}	-0.13	0.79	
I_{04}	-0.44	0.81	
I_{05}	0.11	0.90	
I_{06}	-0.45	0.77	
I_{07}	0.14	0.95	
I_{08}	-0.16	0.84	
I_{09}	-0.32	0.22	
I_{10}	-0.34	0.16	
I_{11}	0.58	0.49	No Distinct Advantage
I_{12}	-0.48	-0.37	

individual taken under varying illumination conditions. Fig. 4 displays the 12 test images of an individual and their respective half-faces with better illumination. We create an eigenspace Φ using a large number of well illuminated frontal faces and an eigenspace Ω using their half-faces. The full-faces and half-faces from the test set are projected on to their respective spaces. Defining a similarity measure between two images based on the correlation between their eigenspace coefficients, we compute the similarity measure between the first test image and the remaining 11 test images. The similarity scores computed using full faces (Set I) and half-faces (Set II) are tabulated in Table III. Half-faces performed better on those image samples where one half of the face was better illuminated, half-faces performed better.

Next, we define a criterion function towards the automatic selection of the better half-faces from regular face images. Given I, a frontal face image of size $m \times n$ we extract I_1 and I_2, the right half and the mirror reflected left half of I. Let $X^i = [x_1, x_2, \ldots\ldots, x_{n/2}]$ denote the column-wise mean intensity of I_i. The mean intensity curve of I_i, $\bar{X}^{(i)}_{\mathrm{MIC}}$ is defined as

$$\bar{X}^{(i)}_{\mathrm{MIC}} = \frac{(X^{(i)} - \bar{X}^{(i)})}{\| X^{(i)} - \bar{X}^{(i)} \|} \tag{11}$$

where $\bar{X}^{(i)}$ denotes the mean of $X^{(i)}$ and $\| \cdot \|$ denotes the Euclidean norm. The difference between the mean intensity curves of either halves of the face is a measure of the disparity in the spread of illumination between the two halves of the face

$$\mathrm{MIC}_d = \| \bar{X}^{(1)}_{\mathrm{MIC}} - \bar{X}^{(2)}_{\mathrm{MIC}} \|. \tag{12}$$

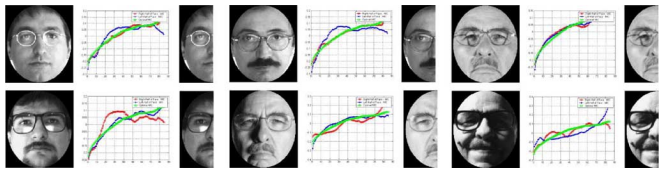

Fig. 5. Half-faces selection criterion. Green: Optimal mean intensity curve. Red: Mean intensity curve from the right half of the face. Blue: Mean intensity curve from the mirror reflected left half of the face. Some of the images from the AR face database [44] were used for illustration purposes.

A low MIC_d indicates that the spread of illumination across either halves of the face is comparable.

Next, using the above measure we compute the *optimal mean intensity curve* for frontal face images. We compute the MIC_d on face images from a large gallery of faces. If $\mathrm{MIC}_d < \alpha$, where α is a predefined threshold, then the face image is classified as optimally illuminated. From N such optimally illuminated face images, we compute the *optimal mean intensity curve* as

$$\bar{X}_{\mathrm{OptimalMIC}} \triangleq \frac{1}{2N} \sum_{i=1}^{N} (\bar{X}^{(1)}_{\mathrm{MIC_i}} + \bar{X}^{(2)}_{\mathrm{MIC_i}}). \tag{13}$$

The criterion function for the selection of the better half face is defined as follows:

$$j = \min_{i=1,2} \| \bar{X}_{\mathrm{OptimalMIC}} - \bar{X}^{(i)}_{\mathrm{MIC}} \| \tag{14}$$

$$I_{\mathrm{opt}} = I_j. \tag{15}$$

Fig. 5 illustrates the mean intensity curves for both halves of faces under different illumination conditions.

III. AGE DIFFERENCE CLASSIFIER

In this section, we develop an age difference classifier designed primarily for the purpose of establishing the identity between a pair of age separated face images and for estimating the age separation between the pair of face images. It has been observed that while faces undergo significant variations in shape from infancy to teenage years, they undergo considerably lesser variations in shape during adulthood. During adulthood, aging effects in faces are more commonly observed in the form of textural variations such as wrinkles and other skin artifacts. Facial wrinkles are primarily attributed to factors such as loss of skin elasticity (due to lesser production of collagen), habitual facial expressions, effects of gravity on facial muscles, over exposure to sun's rays, etc.

Since the database of passport images comprises of individuals in the age range (20 years to 70 years), the age difference classifier is developed primarily to verify adult face images across age progression. Hence, in our formulation the age-difference based classification of face images is based on textural variations that are commonly observed in faces due to aging. Across each pair of face images, we compute the difference image by subtracting the more recent image from the older image. The difference image, when computed between age separated images of the same individual (intrapersonal images),

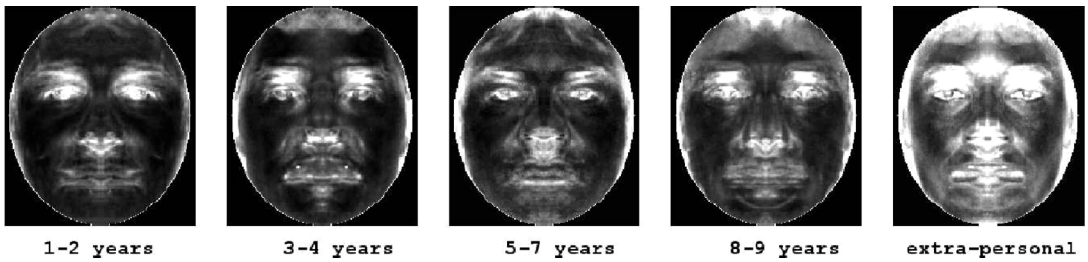

Fig. 6. Average difference images from the intrapersonal (under each of the four age-difference categories) and extrapersonal classes.

captures facial variations due to aging effects. Intuitively, the difference images obtained from the intrapersonal image pairs (image pairs of the same individual) with smaller age separation would be less exaggerated than that obtained from the intrapersonal image pairs with larger age separation. Further, one would expect the difference images obtained from images belonging to different individuals (extrapersonal images) to be different from the ones obtained from intrapersonal images due to the large mismatch in facial features. Fig. 6 illustrates the average difference images computed from intrapersonal images with an age separation of 1–2 years, 3–4 years, 5–7 years, 8–9 years, and that computed from extrapersonal images. The sagging of facial features becomes prominent in the average difference images obtained from intrapersonal images as the age difference increases. Prior to classification of faces based on age differences, we perform the preprocessing steps discussed in the previous section to reduce variations due to pose and illumination.

A. Bayesian Framework

We propose a Bayesian age-difference classifier that is built on a probabilistic eigenspaces framework [45]. The framework proposed in [45] was adopted primarily to estimate complex density functions in high-dimensional image spaces and subsequently to compute class conditional density functions. The classification of pairs of face images based on their age-differences, consists of two stages. In the first stage of classification, the identity between the pair of face images is established. In the second stage, the pairs of age separated face images that were identified as intrapersonal images are further classified based on their age differences.

Let Ω_I denote the intrapersonal space and let Ω_E denote the extrapersonal space. Let $I_{11}, I_{12}, I_{21}, I_{22}, \ldots, I_{M1}, I_{M2}$ be the set of $N \times 1$ vectors formed by the lexicographic ordering of pixels in each of the M pairs of half-faces. The intrapersonal image differences $\{\mathbf{x}_i\}_{i=1}^{M}$ are obtained by the difference of individuals' pairs of half-faces

$$\mathbf{x}_i = I_{i1} - I_{i2},\ 1 \leq i \leq M. \tag{16}$$

The extrapersonal image differences $\{\mathbf{z}_i\}_{i=1}^{M}$ are obtained by the difference of half-faces of different individuals

$$\mathbf{z}_i = I_{i1} - I_{j2}\ ,\ j \neq i,\ 1 \leq i, j \leq M. \tag{17}$$

First, from a set of intrapersonal image differences $\{\mathbf{x}_i\}_{i=1}^{M} \in \Omega_I$, we estimate the likelihood function for the data $P(\mathbf{x}_i|\Omega_I)$. We assume the intrapersonal difference images to be Gaussian distributed. Upon performing a Karhunen Loeve Transform [46] on the training data we get the basis vectors $\{\Phi_i\}_{i=1}^{N}$ that span the intrapersonal space. But due to the high dimensionality of data such a computation is infeasible. We perform PCA [34] and extract the k basis vectors $\{\Phi_i\}_{i=1}^{k}$ that capture 99% variance in the data. The space spanned by $\{\Phi_i\}_{i=1}^{k}$ corresponds to the principal subspace or the feature space F. The remaining basis vectors $\{\Phi_i\}_{i=k+1}^{N}$ span the orthogonal complement space or the error space $\bar{F}$. The likelihood function $P(x_i|\Omega_I)$ is estimated as

$$\begin{aligned} P(\mathbf{x}|\Omega_I) &= \frac{\exp\left(-\frac{1}{2}(\mathbf{x}-\bar{\mathbf{x}})^T\Sigma^{-1}(\mathbf{x}-\bar{\mathbf{x}})\right)}{(2\pi)^{N/2}|\Sigma|^{1/2}} \\ &= \frac{\exp\left(-\frac{1}{2}\sum_{i=1}^{N}\frac{y_i^2}{\lambda_i}\right)}{(2\pi)^{N/2}\prod_{i=1}^{N}\lambda_i^{1/2}} \\ &\simeq \left[\frac{\exp\left(-\frac{1}{2}\sum_{i=1}^{k}\frac{y_i^2}{\lambda_i}\right)}{(2\pi)^{k/2}\prod_{i=1}^{k}\lambda_i^{1/2}}\right] \cdot \left[\frac{\exp\left(-\frac{\epsilon^2(\mathbf{x})}{2\rho}\right)}{(2\pi\rho)^{(N-M)/2}}\right] \\ &= P_F(\mathbf{x}|\Omega_I) \cdot \hat{P}_{\bar{F}}(\mathbf{x}|\Omega_I) \end{aligned} \tag{18}$$

where $y_i = \Phi_i^T(x - \bar{x})$ are the principal component feature vectors and λ_i are the eigenvalues. The marginal density in the orthogonal complement space $\hat{P}_{\bar{F}}(\mathbf{x}|\Omega_I)$ is estimated using the error in PCA reconstruction $\epsilon^2(\mathbf{x}) = \|\tilde{\mathbf{x}}^2\| - \sum_{i=1}^{k} y_i^2$ and the estimated variance along each dimension in the orthogonal subspace, $\rho = (1/(N-k))\sum_{i=k+1}^{N}\lambda_i$. The sum $\sum_{i=k+1}^{N}\lambda_i$ is estimated by fitting a cubic spline function on the computed eigenvalues $\{\lambda_i\}_{i=1}^{k}$ and subsequently extrapolating the function.

Next, from a set of extrapersonal image differences $\{\mathbf{z}_i\}_{i=1}^{M} \in \Omega_E$, we estimate the likelihood function $P(\mathbf{z}_i|\Omega_E)$. Adopting a similar approach as before, the extrapersonal space is decomposed into two complementary spaces: the feature space and the error space. Since the assumption of Gaussian distribution of extrapersonal image differences may not hold, we adopt a parametric mixture model (mixture of Gaussian) to estimate the marginal density in the feature space and follow a similar approach to estimate the marginal density in the

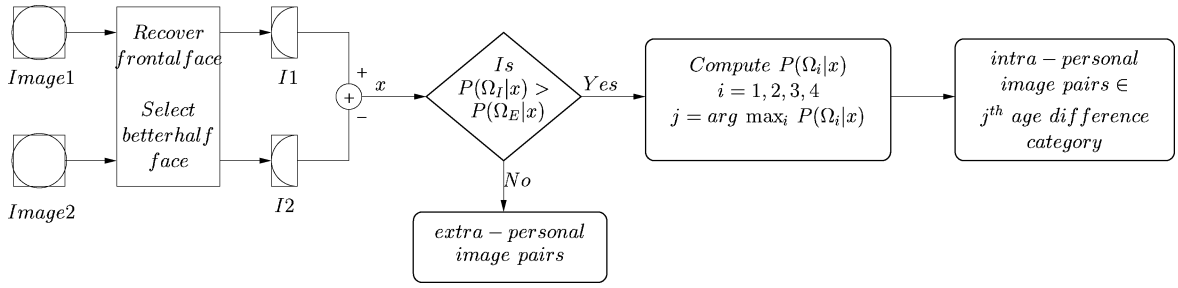

Fig. 7. Overview of the Bayesian age-difference classifier.

orthogonal complement space. We estimate the likelihood for the data as

$$\hat{P}(\mathbf{z}|\Omega_E) = P(\mathbf{y}|\Theta^*) \cdot \hat{P}_{\bar{F}}(\mathbf{z}|\Omega_E)$$

where

$$P(\mathbf{y}|\Theta) = \sum_{i=1}^{N_c} w_i N(\mathbf{y}; \mu_i, \Sigma_i) \tag{19}$$

$$\Theta^* = \arg\max \left[\prod_{i=1}^{M} P(\mathbf{y}_i|\Theta) \right]. \tag{20}$$

$N(\mathbf{y}; \mu_i, \Sigma_i)$ is Gaussian with parameters (μ_i, Σ_i) and w_i correspond to the mixing parameters such that $\sum_{i=1}^{N_c} w_i = 1$. We solve the estimation problem using the expectation-maximization algorithm [47].

During the first stage of classification, given a pair of age separated face images, we extract the well illuminated half-faces I_1 and I_2 and compute the difference image $\mathbf{x} = I_1 - I_2$. The *a posteriori* probability $P(\Omega_I|\mathbf{x})$ is computed using the Bayes rule

$$P(\Omega_I|\mathbf{x}) = \frac{P(\mathbf{x}|\Omega_I)P(\Omega_I)}{P(\mathbf{x}|\Omega_I)P(\Omega_I) + P(\mathbf{x}|\Omega_E)P(\Omega_E)}. \tag{21}$$

The classification of the image difference as intrapersonal or extrapersonal is based on a maximum *a posteriori* (MAP) rule. For operational conditions, $P(\Omega_I)$ and $P(\Omega_E)$ are set equal and the difference image $\mathbf{x}$ is classified as intra personal if $P(\Omega_I|\mathbf{x}) > 1/2$.

The second stage of classification deals with classifying the intrapersonal image pairs into one of many age difference categories. For each of the four age-difference categories (1–2 years, 3–4 years, 5–7 years, and 8–9 years), we build the intrapersonal spaces denoted as Ω_1, Ω_2, Ω_3, Ω_4. Next, from a set of age-difference based intrapersonal difference images we estimate the likelihood function $P(\mathbf{x}|\Omega_j)$, j ∈ 1, 2, 3, 4 for each of the four age-difference categories. Given a difference image $\mathbf{x}$ that has been classified as intrapersonal, we compute the *a posteriori* probability $P(\Omega_i|\mathbf{x})$ with $i = 1, 2, 3, 4$ as

$$P(\Omega_i|\mathbf{x}) = \frac{P(\mathbf{x}|\Omega_i)P(\Omega_i)}{\sum_{j=1}^{4} P(\mathbf{x}|\Omega_j)P(\Omega_j)}. \tag{22}$$

Thus, if $P(\Omega_i|\mathbf{x}) > P(\Omega_j|\mathbf{x})$ for all $j \neq i$, $i, j = 1, 2, 3, 4$, then Ω_i is identified to be the class to which the difference image $\mathbf{x}$ belongs. Fig. 7 gives a complete overview of the age-difference classifier.

B. Experiments and Results

Using the above formulation, we performed classification experiments on the passport database. We selected pairs of better illuminated half-faces of 200 individuals from the database. Using their intrapersonal image differences, we created the intrapersonal space Ω. Computing the extra personal difference images (by randomly selecting two images of different individuals from the 200 pairs of images) we created the extrapersonal space Ψ. We created two sets of image differences: Set I comprised of intrapersonal difference images computed from the half-faces of 465 image pairs from the database and Set II comprised of 465 extrapersonal difference images computed by a random selection of half-faces of different individuals from the database. The image pairs from Set I and Set II were classified as either intrapersonal or extrapersonal.

During the second stage of classification, 50 pairs of half-face images from each of the following age-difference categories 1–2 years, 3–4 years, 5–7 years, and 8–9 years were randomly selected and their corresponding difference image subspaces namely, Ω_1, Ω_2, Ω_3, Ω_4, were created. The image pairs from Set I that were classified as intrapersonal were further classified into one of the four age-difference categories using the formulation discussed previously. The classification experiment was repeated many times using different sets of images from each age-difference category to create the intrapersonal spaces. The classification results are reported in Table IV in the form of percentage of images under each category that were classified into one of the four classes. The means and the standard deviations of the classification results generated from the many iterations are reported in Table IV. The bold entries in the table correspond to the percentage of image pairs that were correctly classified to their age-difference category. The entries within parenthesis denote the standard deviations.

The classification results can be summarized as follows.

- At the operating point, 99% of the difference images from Set I were correctly classified as intrapersonal. 83% of the difference images from Set II were correctly classified as extrapersonal. It was observed that the image pairs from Set I that were misclassified as extrapersonal differed from each other significantly either in facial hair or glasses. Moreover, the average age difference of intrapersonal images that were misclassified was 7.4 years. The ROC plot

TABLE IV
OVERALL RESULTS OF THE BAYESIAN AGE-DIFFERENCE CLASSIFIER

Type	Class	1-2 yrs	3-4 yrs	5-7 yrs	8-9 yrs
Original set of images	Ω_1	**41.0 (1.1)**	12.0 (6.9)	9.0 (5.0)	38.0 (7.2)
	Ω_2	8.0 (5.0)	**46.0 (5.6)**	8.0 (4.9)	37.0 (9.2)
	Ω_3	10.0 (3.3)	8.0 (6.3)	**53.0 (4.4)**	28.0 (6.9)
	Ω_4	10.0 (2.3)	12.0 (7.3)	5.0 (5.4)	**73.0 (8.2)**

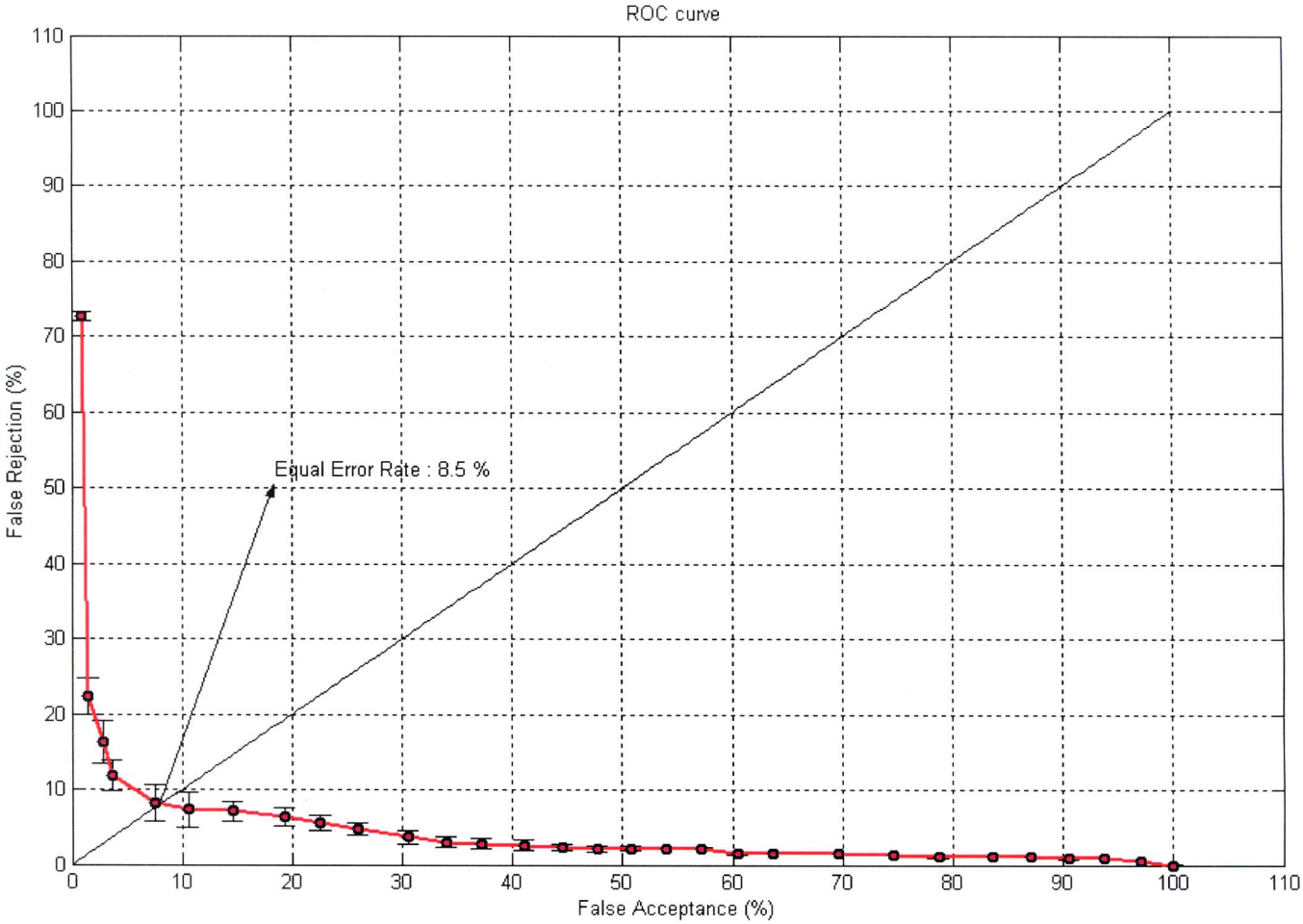

Fig. 8. Face verification results: ROC curve. (Color version available online at http://ieeexplore.ieee.org.)

in Fig. 8 was generated by varying the thresholds adopted for classification. The equal error rate is 8.5%.

- When the image pairs from Set I that were correctly classified as intrapersonal were classified further based on age-differences, it was observed that image pairs with little variations due to factors such as facial expressions, glasses and facial hair were more often classified correctly to their respective age-difference category.
- Image pairs, that belong to the age difference categories 1–2 years or 3–4 years or 5–7 years, with significant differences in facial hair or expressions or glasses, were misclassified under the category 8–9 years. Since Ω_4 was built using images from the age difference category 8–9 years, it spans more intra pair variations than those compared with the other three age difference categories, and, hence, the above trend is observed.

To study the effects of external variations, such as facial hair, glasses, and facial expressions on classification accuracy, images with such variations were identified and classified separately. The images from the database were divided into four sets—ones with differences in facial hair, differences in glasses, differences in facial expressions and finally, ones with little external variations (henceforth, addressed as nonvariate images). Those images with variations due to multiple external factors were classified based on the most dominant factor that caused the variations. Classification results for nonvariate images are reported in Table V. The classification results on images pairs with variations in facial expressions, glasses, facial hair are reported in Tables VI–VIII, respectively.

- A comparison of the classification results in Tables IV and V highlights the bias introduced by external factors such as facial hair, glasses and facial expression on age-difference

TABLE V
CLASSIFICATION RESULTS ON NON-VARIATE IMAGES PAIRS

Type	Class	1-2 yrs	3-4 yrs	5-7 yrs	8-9 yrs
Images with less external variations	Ω_1	**53.0 (3.8)**	14.0 (2.3)	12.0 (5.0)	21.0 (7.2)
	Ω_2	9.0 (3.0)	**53.0 (4.0)**	10.0 (6.1)	29.0 (8.0)
	Ω_3	11.0 (4.9)	8.0 (4.5)	**62.0 (2.9)**	19.0 (7.2)
	Ω_4	14.0 (4.3)	13.0 (6.5)	6.0 (6.1)	**67.0 (8.9)**

TABLE VI
CLASSIFICATION RESULTS ON IMAGES PAIRS WITH FACIAL EXPRESSIONS

Type	Class	1-2 yrs	3-4 yrs	5-7 yrs	8-9 yrs
Images with variations in facial expressions	Ω_1	**33.0 (2.7)**	11.0 (14.3)	5.0 (4.9)	51.0 (13.5)
	Ω_2	10.0 (10.0)	**39.0 (9.3)**	9.0 (5.7)	42.0 (12.2)
	Ω_3	13.0 (4.2)	6.0 (8.9)	**57.0 (9.1)**	24.0 (2.0)
	Ω_4	8.0 (4.4)	12.0 (6.5)	6.0 (4.1)	**74.0 (8.9)**

TABLE VII
CLASSIFICATION RESULTS ON IMAGES PAIRS WITH GLASSES

Type	Class	1-2 yrs	3-4 yrs	5-7 yrs	8-9 yrs
Images with variations in glasses	Ω_1	**25.0 (1.9)**	12.0 (10.5)	5.0 (9.9)	58.0 (11.9)
	Ω_2	4.0 (5.2)	**51.0 (7.6)**	5.0 (6.7)	40.0 (6.7)
	Ω_3	9.0 (3.1)	8.0 (9.1)	**42.0 (6.4)**	41.0 (10.6)
	Ω_4	9.0 (2.9)	9.0 (10.3)	3.0 (7.2)	**79.0 (11.3)**

TABLE VIII
CLASSIFICATION RESULTS ON IMAGES PAIRS WITH FACIAL HAIR

Type	Class	1-2 yrs	3-4 yrs	5-7 yrs	8-9 yrs
Images with variations in facial hair	Ω_1	**28.0 (4.6)**	7.0 (12.9)	5.0 (7.5)	60.0 (18)
	Ω_2	6.0 (8.2)	**41.0 (9.0)**	9.0 (5.2)	42.0 (10.7)
	Ω_3	2.0 (2.8)	12.0 (15.9)	**48.0 (6.3)**	38.0 (12.1)
	Ω_4	5.0 (2.4)	11.0 (7.6)	4.0 (4.2)	**80.0 (7.4)**

based classification. While classification results improved in the age-difference categories 1–2 years, 3–4 years, and 5–6 years on image pairs with little variations, classification results in the 8–9 years category were less accurate when compared to that obtained on the original image set.

- As observed in Tables VI–VIII, age-difference based classification suffers heavily in the presence of factors such facial hair, glasses, and facial expressions. Since the variations induced by these factors mask variations due to aging effects, image pairs with lower age-differences were more often classified into the age-difference category 8–9 years.

The eigenspace decomposition which forms an inherent part of the density estimation process reduces computational complexities significantly. Further, since the estimation of the class conditional density functions is an off-line process, the real-time computations involved in classifying image pairs based on age differences are simple.

IV. SIMILARITY MEASURE

We designed the following experiment to study how age progression affects the measure of facial similarity. We created an eigenspace using 200 half-faces retrieved from the database of passport images. The 465 pairs of half-faces were projected onto the space of eigenfaces and were represented by the projections along the eigenfaces that correspond to 95% of the variance. We adopt the similarity measure proposed in Section II. Since illumination and pose variations across each pair of half-faces is minimal, the similarity score between each pair would be affected by factors such as age progression, facial expression variations and occlusions due to facial hair and glasses. We divided our database into two sets: the first set comprised of those images where each pair of passport images had similar facial expressions and similar occlusions if any, due to glasses and facial hair. The second set comprised of those pairs of passport images where differences due to facial expressions or occlusions due to glasses and facial hair were significant.

The distribution of similarity scores across the age-difference categories 1–2 years, 3–4 years, 5–7 years, and 8–9 years, is plotted in Fig. 9. The statistical variations in the similarity scores across each age-difference category and across each set of passport images are tabulated in Table IX.

- From Fig. 9, we note that as the age difference between the pairs of images increases, the proportion of images with high similarity scores decreases.
- While the distribution of similarity scores has a strong peak for category 1–2 years, it flattens out gradually as the age difference increases.

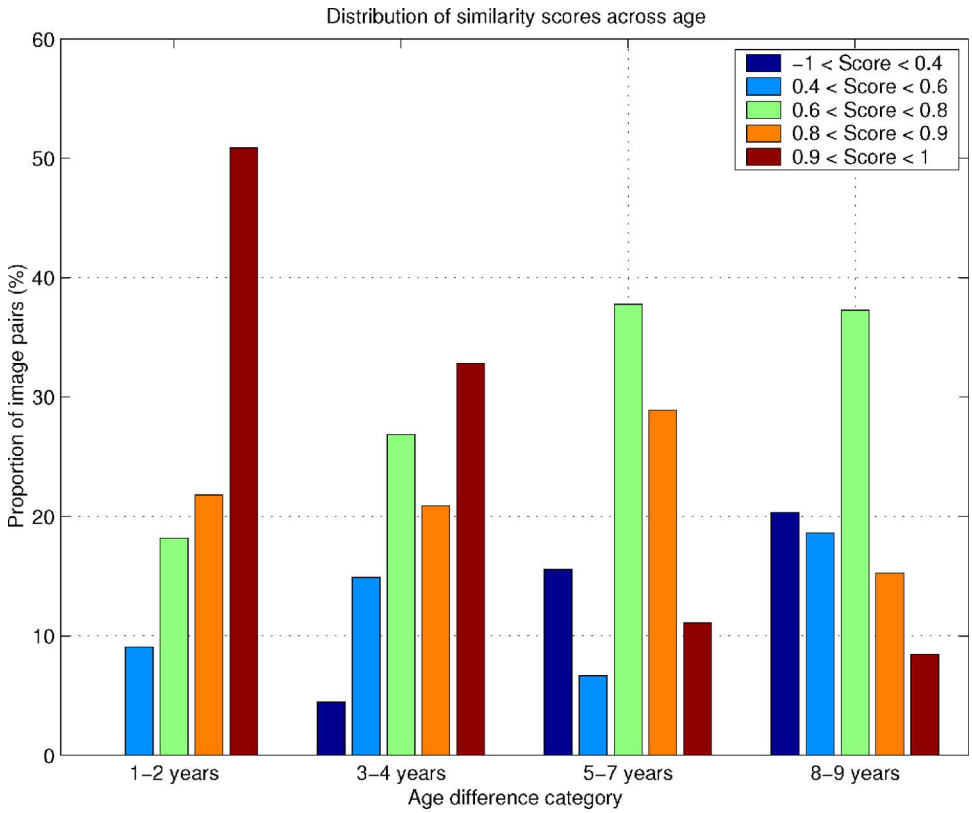

Fig. 9. Facial similarity across time: Distribution of similarity scores across age. (Color version available online at http://ieeexplore.ieee.org.)

TABLE IX
SIMILARITY MEASURE

Age Based Similarity Measure								
Age Difference	First Set		Second Set					
			Expression		Glasses		Facial Hair	
	μ	σ^2	μ	σ^2	μ	σ^2	μ	σ^2
1-2 yrs	0.85	0.02	0.70	0.021	0.83	0.01	0.67	0.04
3-4 yrs	0.77	0.03	0.65	0.07	0.75	0.02	0.63	0.01
5-7 yrs	0.70	0.06	0.59	0.01	0.72	0.02	0.59	0.10
8-9 yrs	0.60	0.08	0.55	0.10	0.68	0.18	0.55	0.10

- From Table IX, we note that as the age difference increases, across both the sets of images and across all the variations such as expressions, glasses and facial hair, the mean similarity score drops gradually and the variance of the similarity scores increases.
- Within each age-difference category, we see a notable drop in similarity scores when variations due to expressions and facial hair are more pronounced.

V. DISCUSSIONS AND CONCLUSION

From a face recognition perspective, understanding the process of age progression in human faces is crucial towards the development of face recognition systems that are robust to aging effects and in the successful deployment of such systems. Some of the limitations one faces while addressing age progression in human faces as discussed as follows.

- Modeling the complex shape variations human faces undergo during one's younger years or the textural variations that are observed during the later years is a very challenging task. Apart from biological factors, since factors as diverse as ethnicity, climatic conditions, food intake, mental stress, etc., also contribute towards aging effects, it is natural to expect different individuals to age differently.
- Manifestations of aging effects in human faces such as shape and textural variations can be best understood using 3-D scans of human heads. With 3-D head scans becoming increasingly available, we anticipate the development of more robust methods to address age progression in the future.
- Lack of databases of age progressed face images of individuals is another reason for lesser research on this topic. Only recently, the FG-Net aging database [48] that contains real life images of many individuals across ages, has

become publicly available. Since real life images are often taken under uncontrolled environments, the age separated images in this database differ significantly in other aspects such as illumination and pose. Such external variations need to be minimized before studying aging effects.

Our primary objective was to study the effects of age progression on facial similarity measure and to develop systems that can perceive age separation between a pair of images of an individual. The relatively well-controlled environments under which passport images are taken, make them ideally suited for studying the effects of age progression in human faces. We presented a Bayesian age-difference classifier that identifies the age separation between a pair of face images of an individual. In our formulation, the difference images obtained from a pair of intrapersonal age separated face images formed the primary basis for classification. While the characterization of the intrapersonal difference images were based on their age differences, the age group to which the image pairs belonged to, were not considered primarily due to lack of sufficient samples to characterize such variations for each age group. While the method presented in this paper is suitable to handle age progression in adult face images, since it does not account for shape variations in faces, it may not be effective for handling age progression in face images of children. We also studied facial similarity across age progression and highlighted the role of age progression in affecting similarity scores. The methods presented to address age progression in human faces have direct relevance to passport image renewal applications.

ACKNOWLEDGMENT

The authors would like to thank Dr. A. K. R. Chowdhury and Dr. D. Jacobs for many interesting discussions on this topic. They would also like to thank T. Mendez for providing them with his disguised images.

REFERENCES

[1] N. Ramanathan and R. Chellappa, "Face verification across age progression," in *Proc. IEEE Conf. Computer Vision and Pattern Recognition*, San Diego, CA, 2005, vol. 2, pp. 462–469.

[2] W.-Y. Zhao, R. Chellappa, P. J. Phillips, and A. Rosenfeld, "Face recognition: A literature survey," *ACM Comput. Surv.*, vol. 35, no. 4, pp. 399–458, Dec. 2003.

[3] L. Zhang and D. Samaras, "Face recognition from a single training image under arbitrary unknown lighting using spherical harmonics," *IEEE Trans. Pattern Anal. Mach. Intell.*, vol. 28, no. 3, pp. 351–363, Mar. 2006.

[4] S. K. Zhou and R. Chellappa, "Image-based face recognition under illumination and pose variations," *J. Opt. Soc. Amer.*, vol. 22, pp. 217–229, Feb. 2005.

[5] V. Blanz and T. Vetter, "Face recognition based on fitting a 3D morphable model," *IEEE Trans. Pattern Anal. Mach. Intell.*, vol. 25, no. 9, pp. 1063–1074, Sep. 2003.

[6] A. S. Georghiades, P. N. Belhumeur, and D. J. Kriegman, "From few to many: Illumination cone models for face recognition under variable lighting and pose," *IEEE Trans. Pattern Anal. Mach. Intell.*, vol. 23, no. 6, pp. 643–660, Jun. 2001.

[7] R. Gross, S. Baker, I. Matthews, and T. Kanade, "Face recognition across pose and illumination," in *Handbook of Face Recognition*. New York: Springer, 2004.

[8] P. Ekman and W. Friesen, *Facial Action Coding System: A Technique for the Measurement of Facial Movement*. Consulting Psychologists Press .

[9] Y. Yacoob and L. Davis, "Recognizing human facial expressions from long image sequences using optical flow," *IEEE Trans. Pattern Anal. Mach. Intell.*, vol. 18, no. 6, pp. 636–642, Jun. 1996.

[10] I. Essa and A. Pentland, "Coding, analysis, interpretation and recognition of facial expressions," *IEEE Trans. Pattern Anal. Mach. Intell.*, vol. 19, no. 7, pp. 757–763, Jul. 1997.

[11] A. M. Martinez, "Matching expression variant faces," *Vis. Res.*, vol. 43, pp. 1047–1060, 2003.

[12] Y.-L. Tian, T. Kanade, and J. F. Cohn, "Facial expression analysis," in *Handbook of Face Recognition*. New York: Springer, 2004.

[13] Y. Liu, K. L. Schmidt, J. F. Cohn, and S. Mitra, "Facial asymmetry quantification for expression invariant human identification," *Comput. Vis. Image Understand.*, vol. 91, no. 1/2, pp. 138–159, Jul. 2003.

[14] P. J. Phillips, H. Moon, S. A. Rizvi, and P. J. Rauss, "The FERET evaluation methodology for face-recognition algorithms," *IEEE Trans. Pattern Anal. Mach. Intell.*, vol. 22, no. 10, pp. 1090–1104, Oct. 2000.

[15] S. A. Rizvi, P. J. Phillips, and H. Moon, "The FERET verification protocol and statistical performance analysis for face recognition algorithm," in *IEEE Conf. Computer Vision and Pattern Recognition*, 1998, pp. 833–838.

[16] P. Phillips, P. Grother, R. Micheals, D. Blackburn, E. Tabassi, and J. Bone, "Frvt 2002: Overview and Summary," Tech. Rep. 2003 [Online]. Available: http://www.frvt.org

[17] L. S. Mark, R. E. Shaw, and J. B. Pittenger, "Natural constraints, scales of analysis, and information for the perception of growing faces," in *Social and Applied Aspects of Perceiving Faces*. Mahwah, NJ: Lawrence Erlbaum, 1998.

[18] E. J. Gibson, *Principles of Perceptual Learning and Development*. New York: Appleton-Century-Crofts, 1969.

[19] D. W. Thompson, *On Growth and Form*. New York: Dover, 1992.

[20] R. E. Shaw, M. McIntyre, and W. Mace, "The role of symmetry in event perception," *Perception: Essays in Honor of James J. Gibson*, pp. 276–310, 1974.

[21] J. B. Pittenger and R. E. Shaw, "Aging faces as viscal-elastic events: Implications for a theory of nonrigid shape perception," *J. Exp. Psych.: Human Perception and Performance*, vol. 1, no. 4, pp. 374–382, 1975.

[22] J. T. Todd, L. S. Mark, R. E. Shaw, and J. B. Pittenger, "The perception of human growth," *Sci. Amer.*, vol. 242, no. 2, pp. 132–144, 1980.

[23] Y. H. Kwon and N. da Vitoria Lobo, "Age classification from facial images," *Comput. Vis. Image Understand.*, vol. 74, pp. 1–21, Apr. 1999.

[24] A. Lanitis, C. J. Taylor, and T. F. Cootes, "Toward automatic simulation of aging effects on face images," *IEEE Trans. Pattern Anal. Mach. Intell.*, vol. 24, no. 4, pp. 442–455, Apr. 2002.

[25] A. Lanitis, C. Draganova, and C. Christodoulou, "Comparing different classifiers for automatic age estimation," *IEEE Trans. Syst., Man, Cybern.. B, Cybern.*, vol. 34, no. 1, pp. 621–628, Feb. 2004.

[26] M. Burt and D. I. Perrett, "Perception of age in adult caucasian male faces: Computer graphic manipulation of shape and colour information," *J. Roy. Soc.*, vol. 259, pp. 137–143, Feb. 1995.

[27] B. Tiddeman, D. M. Burt, and D. Perret, "Prototyping and transforming facial texture for perception research," *IEEE Comput. Graph. Appl.*, vol. 21, no. 5, pp. 42–50, Jul.-Aug. 2001.

[28] Y. Wu, N. Thalmann, and D. Thalmann, "A dynamic wrinkle model in facial animation and skin aging," *J. Vis. Comput. Animation*, vol. 6, pp. 195–205, 1995.

[29] A. J. O'Toole, T. Vetter, H. Volz, and M. Salter, "Three-dimensional caricatures of human heads: Distinctiveness and the perception of facial age," *Perception*, vol. 26, pp. 719–732, 1997.

[30] M. Gandhi, "A Method for Automatic Synthesis of Aged Human Facial Images," M.S. thesis, McGill Univ., Montreal, QC, Canada, 2004.

[31] Y. Shan, Z. Liu, and Z. Zhang, "Image based surface detail transfer," in *Proc. IEEE Conf. Computer Vision and Pattern Recognition*, 2001, vol. 2, pp. 794–799.

[32] G. H. Givens, J. R. Beveridge, B. A. Draper, P. Grother, and P. J. Phillips, "How features of the human face affect recognition: A statistical comparison of three face recognition algorithms," in *Proc. Int. Conf. Pattern Recognition*, 2004, vol. 2, pp. 381–388.

[33] V. Blanz and T. Vetter, "A morphable model for the synthesis of 3D faces," in *Proc. SIGGRAPH*, 1999, pp. 187–194.

[34] D. G. S. Richard, O. Duda, and P. E. Hart, *Pattern Classification*, 2nd ed. New York: Wiley, 2001.

[35] M. J. Jones and J. M. Regh, "Statistical color models with application to skin detection," *Int. J. Comput. Vis.*, vol. 46, no. 1, pp. 81–96, Jan. 2002.

[36] P. N. Belhumeur, J. P. Hespanha, and D. J. Kriegnan, "Eigenfaces vs. fisherfaces: Recognition using class specific linear projection," *IEEE Trans. Pattern Anal. Mach. Intell.*, vol. 19, no. 7, pp. 711–720, Jul. 1997.
[37] R. Basri and D. W. Jacobs, "Lambertial reflectance and linear subspaces," *IEEE Trans. Pattern Anal. Mach. Intell.*, vol. 25, no. 2, pp. 218–233, Feb. 2003.
[38] K.-C. Lee, J. Ho, and D. J. Kriegman, "Acquiring linear subspaces for face recognition under variable lighting," *IEEE Trans. Pattern Anal. Mach. Intell.*, vol. 27, no. 5, pp. 684–698, May 2005.
[39] G. Aggarwal and R. Chellappa, "Face recognition in the presence of multiple light sources," in *IEEE Int. Conf. Computer Vision*, Beijing, China, Oct. 2005, pp. 1169–1176.
[40] W.-Y. Zhao and R. Chellappa, "Symmetric shape from shading using self ratio images," *Int. J. Comput. Vis.*, vol. 45, pp. 55–75, 2001.
[41] N. Troje and H. Bulthoff, "How is bilateral symmetry of human faces used for recognition of novel views," *Vis. Res.*, vol. 38, no. 1, pp. 79–89, 1998.
[42] A. M. Martinez, "Recognizing imprecisely localized, partially occluded and expression variant faces from a single sample per class," *IEEE Trans. Pattern Anal. Mach. Intell.*, vol. 24, no. 6, pp. 748–763, Jun. 2002.
[43] T. Sim, S. Baker, and M. Bsat, "The CMU pose illumination and expression database," *IEEE Trans. Pattern Anal. Mach. Intell.*, vol. 25, no. 12, pp. 1615–1618, Dec. 2003.
[44] A. M. Martinez and R. Benavente, "The AR Face Eatabase CVC," Tech. Rep., 1998.
[45] B. Moghaddam and A. Pentland, "Probabilistic visual learning for object representation," *IEEE Trans. Pattern Anal. Mach. Intell.*, vol. 19, no. 7, pp. 696–710, Jul. 1997.
[46] M. Loeve, *Probability Theory*. New York: Von Nostrand, 1955.
[47] G. McLachlan and T. Krishnan, *The EM Algorithm and Extensions*. New York: Wiley, 1996.
[48] *FG-Net Aging Database*, [Online]. Available: http://sting.cycollege.ac.cy/~alanitis/fgnetaging/

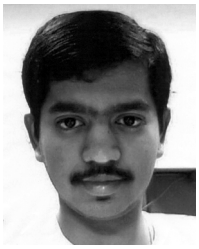

Narayanan Ramanathan received the B.E.(Hons) degree in electrical and electronics engineering from the Birla Institute of Technology and Science, Pilani, in 2002, and the M.S. degree in electrical and computer engineering from the University of Maryland, College Park, in 2004, where he is currently pursuing Ph.D degree in electrical and computer engineering.

His research interests span computer vision, pattern recognition, and image processing. He was awarded the university gold medal for the Batch of 2002 from the Birla Institute of Technology and Science.

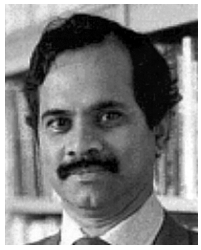

Rama Chellappa (S'78–M'79–SM'83–F'92) received the B.E. (Hons.) degree from the University of Madras, Madras, India, in 1975 and the M.E. (Distinction) degree from the Indian Institute of Science, Bangalore, in 1977. He received the M.S.E.E. and Ph.D. degrees in electrical engineering from Purdue University, West Lafayette, IN, in 1978 and 1981, respectively.

Since 1991, he has been a Professor of electrical engineering and an affiliate Professor of Computer Science at the University of Maryland, College Park. Recently, he was named the Minta Martin Professor of Engineering. He is also affiliated with the Center for Automation Research (Director) and the Institute for Advanced Computer Studies (permanent member). Prior to joining the University of Maryland, he was an Assistant Professor (1981 to 1986) and an Associate Professor (1986 to 1991) and Director of the Signal and Image Processing Institute (1988 to 1990) with the University of Southern California (USC), Los Angeles. Over the last 25 years, he has published numerous book chapters and peer-reviewed journal and conference papers. He has also coedited and coauthored many research monographs. His current research interests are face and gait analysis, 3-D modeling from video, automatic target recognition from stationary and moving platforms, surveillance and monitoring, hyperspectral processing, image understanding, and commercial applications of image processing and understanding.

Dr. Chellappa has served as an Associate Editor of many IEEE journals. He was a co-Editor-in-Chief of *Graphical models and Image Processing*. He also served as the Editor-in-Chief of the IEEE TRANSACTIONS ON PATTERN ANALYSIS AND MACHINE INTELLIGENCE from 2001 to 2004. He served as a member of the IEEE Signal Processing Society Board of Governors from 1996 to 1999 and as its Vice President of Awards and Membership from 2002 to 2004. He has received several awards, including the National Science Foundation Presidential Young Investigator Award, two IBM Faculty Development Awards, the 1990 Excellence in Teaching Award from School of Engineering at USC, the 1992 Best Industry Related Paper Award from the International Association of Pattern Recognition (with Q. Zheng), and the 2000 Technical Achievement Award from the IEEE Signal Processing Society. He was elected as a Distinguished Faculty Research Fellow (1996 to 1998), and as a Distinguished Scholar-Teacher (2003) at the University of Maryland. He is a Fellow of the International Association for Pattern Recognition. He has served as a General the Technical Program Chair for several IEEE international and national conferences and workshops. He is a Golden Core Member of IEEE Computer Society.